Int J Adv Manuf Technol (2011) 54:431–443
DOI 10.1007/s00170-010-2940-8

ORIGINAL ARTICLE

Analytical prediction of cutting forces in orthogonal cutting using unequal division shear-zone model

Binglin Li · Xuelin Wang · Yujin Hu · Chenggang Li

Received: 2 December 2009 / Accepted: 13 September 2010 / Published online: 16 October 2010

Abstract This paper presents an analytical method based on the unequal division shear-zone model to study the machining predictive theory. The proposed model only requires workpiece material properties and cutting conditions to predict the cutting forces during the orthogonal cutting process. In the shear zone, the material constitutive relationship is described by Johnson–Cook model, and the material characteristics such as strain rate sensitivity, strain hardening, and thermal softening are considered. The chip formation is supposed to occur mainly by shearing within the primary shear zone. The governing equations of chip flow through the primary shear zone are established by introducing a piecewise power law distribution assumption of the shear strain rate. The cutting forces are calculated for different machining conditions and flow stress data. Prediction results were compared with the orthogonal cutting test data from the available literature and found in reasonable agreement. In addition, an analysis of the deviation from experimental data for the proposed model is performed, the effects of cutting parameters and tool geometry were investigated.

Keywords Orthogonal cutting · Cutting force · Machining simulation · Analytical model

B. Li (✉) · X. Wang · Y. Hu · C. Li
Department of Mechanical Design,
School of Mechanical Science and Engineering,
Huazhong University of Science and Technology,
Wuhan, Hubei Province 430074, China
e-mail: lubay600@sina.com

1 Introduction

In metal cutting, cutting force governs cutting heat generation, tool life, and machining accuracy. In the process planning stage, estimation of cutting force is useful for process engineers to calculate power requirements, to select appropriate process parameters, as well as to design better machining tools and fixtures.

At present, many models of cutting force prediction have been developed using empirical [1], analytical [2], and numerical methods [3]. Empirical models are most often used in practice, however, a large amount data must be gathered and stored in the cutting databases to take account of the different conditions of machining (type of process, geometry, and material of the tool, workpiece material, cutting parameters, etc.). Another shortcoming of the databases is that they do not provide physical mechanism on the cutting processes. Typical approaches for numerical modeling are FEM. In recent years, the FEM has particularly become the main tool for simulation of the metal cutting process, and there is software that provides simulation function of the orthogonal cutting [4]. Simulations of FEM are very time consuming and the accuracy of results always need to be improved.

There have been numerous analytical models developed over years for orthogonal cutting. Merchant [5, 6] firstly developed the simplest and most well-known single-shear plane model based on the orthogonal cutting configuration and minimum energy principle. The basic assumption that the deformation occurs on a single-shear plane, produces a velocity discontinuity along which the strain rate is infinite. Although geometric arguments can be used to compute an average effective strain rate, this assumption makes it difficult to include the effect of strain rate hardening, which is known to be a significant factor in high-speed deforma-

tion processes. The single-shear plane model does not consider the effect of strain, strain rate, and temperature on the material property, so when applied to a range of workpiece materials, the model does not provide accurate results.

In re-examining Merchant's theory with regard to shear angle prediction, Oxley [7] subsequently criticized some of the necessary assumptions, considered effects due to strain hardening, strain rate, etc. Oxley and Welsh [8] introduced a new parallel-sided shear-zone model based on direct observations of chip formation. This model had many features of the single-shear plane model, but considered the effects of strain hardening, strain rate, and temperature on the material property. Oxley's theory requires the inputs for flow stress data of the workpiece material that was represented using a power law equation. Unfortunately, such relations are available in the literature for low-carbon steel. Therefore, Adibi-Sedeh et al. [9] and Lalwani et al. [10] extended Oxley's machining theory for prediction of cutting forces and temperatures with other various material models. They found that Johnson and Cook material model performed best in prediction of cutting forces among the different material models. In Oxley's model, the main shear plane is located in the middle of the shear band. Astakhov et al. [11] thought the shear zone can be divided into two unequal parts. Tounsi et al. [12] identified the material coefficients of constitutive equation by using unequal division shear-zone model.

Dudzinski and Molinari [13] developed a thermomechanical model of orthogonal cutting for high-speed machining. They assumed that the hydrostatic pressure was constant in the primary shear zone, and the motion equations reduce to a single relation by calculating the inertial force. Recently, Ozlu et al. [14] modified Dudzinski and Molinari's model by modeling rake contact as sticking and sliding zone in the secondary shear zone, and their respective lengths are also calculated. However, plastic deformation of metal cutting process at general cutting speed are regarded as quasi-static since it is assumed that inertial force due to the plastic flow may be neglected [15].

Up to the present, there is still no research about prediction of orthogonal cutting using unequal division shear-zone model. In this study, an analytical method based on the unequal division shear-zone model for orthogonal cutting is presented. The flow stress in the primary shear zone is represented using Johnson–Cook (JC) material model, taking into consideration the strain, strain rate, and temperature effects. A piecewise power law distribution assumption of the shear strain rate is introduced in order to obtain the governing equation of chip flow through the primary shear zone. Model predictions are compared with orthogonal cutting test data from the available literature for 42CrMo4 Steel [16] and AISI 316L [12].

2 Shear-zone model

With regard to the complexity of the cutting process, which is affected by many factors, it is impossible to present a real model of the primary shear zone. The engineering approach to the characterization of plastic deformation in the shear zone is based on some simplifications including replacing curvilinear boundaries by straight lines. The most commonly used models for the primary shear zone are [17]: (1) Merchant's single-shear plane model; (2) Oxley's parallel-sided shear-zone model; (3) Zorev's pie-shaped shear-zone model, as shown in Fig. 1. In Oxley's model, the main shear plane AB is assumed to open up so the entry boundary CD and the exit boundary EF are parallel to and equidistant from AB, see Fig. 1b. Astakhov et al. [11] thought the shear zone can be divided into two regions, the first part can be called the wide region where the velocity change takes places at a low rate, and the second is the narrow region where this change takes place at a high rate. Astakhov et al. proved that this zone consists of two unequal parts using the microstructure of a single chip fragment, as shown Fig. 2. It is also found that the main shear plane is not located in the middle of the shear band based on a grid deformation in Fig. 3 [18]. Tounsi et al. proposed that the main shear plane AB divided the primary shear-zone into two unequal parts characterized by the portion k according to Astakhove et al. theory, and identified the material coefficients of constitutive equation. In this paper, unequal division shear-zone model is developed to predict the cutting force.

3 Velocity analysis

The velocity diagram is a fundamental issue because it defines the deformation and friction energy spending in the cutting process. Knowing this diagram, all other physical quantities of the cutting process can be defined [12]. In the following, the diagram along with the strain and strain rate fields is determined.

In analyzing the process of metal cutting, the cutting thickness a, the cutting speed V, and the rake angle γ_0 are known. The velocity diagram is shown in the Fig. 4. V_c is the velocity of the chip relative to the tool and directed along the rake face. V_{t0} and V_{th} are the tangential velocity components of the chip directed along the shear plane, V_{n0} and V_{nh} are the normal velocity components of the chip directed along the normal to the shear plane. According to the parallelogram law of velocities, the cutting velocity V is the vector sum of the shear velocity V_{t0} and normal velocity V_{t0} at the entry of the shear zone; the cutting velocity V_c is the vector sum of the shear velocity V_{th} and normal velocity V_{nh} at the exit. We shall restrict this investigation to a one-dimensional approach and steady state flow solution. In the

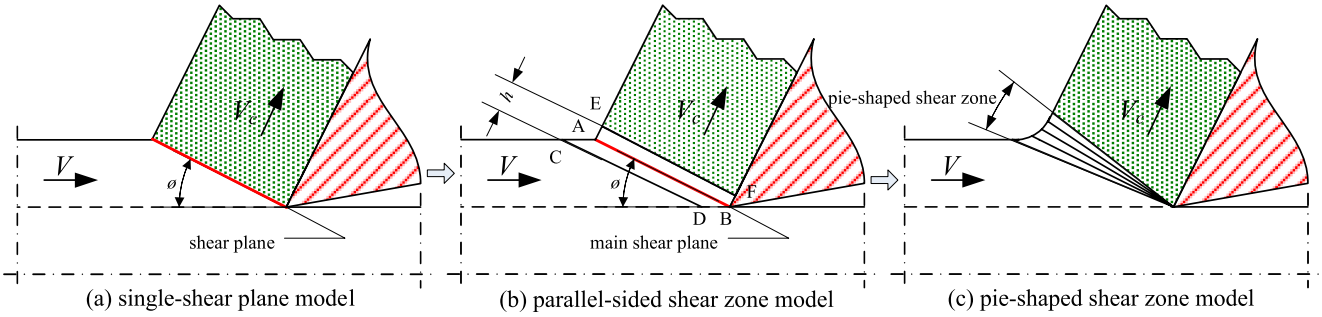

Fig. 1 Simplified models of the primary shear zone

case, all the quantities of the cutting process in the primary shear zone are only dependent on the coordinate y, and the partial time derivative of these quantities vanish. So, the components of the material velocity in the primary zone are defined by

$$\begin{cases} v_x = v_x(y) \\ v_y = v_y(y) \end{cases} \tag{1}$$

The velocity field must satisfy the assumption of plastic incompressibility, consequently, it obeys the following equation.

$$\frac{\partial v_x}{\partial x} + \frac{\partial v_y}{\partial y} = 0 \tag{2}$$

Since the velocity field is expressed as function of y. the equation of plastic incompressibility suggests that the normal velocity component is constant through the primary shear zone.

$$\frac{\partial v_y}{\partial y} = 0 \quad \text{or} \quad v_y = V_n = \text{const} \tag{3}$$

According to the kinetic relations, the tangential and normal velocity components for the boundary conditions are

$$\begin{cases} v_x = v_x(0) = V_{t0} = -V\cos\phi \\ v_x = v_x(h) = V_{th} = V\sin\phi\tan(\phi - \gamma_0) \end{cases} \tag{4}$$

$$\begin{cases} v_y = v_y(0) = V_{n0} = V\sin\phi \\ v_y = v_y(h) = V_{nh} = V_c\cos(\phi - \gamma_0) \end{cases} \tag{5}$$

The difference between the velocities V_{t0} and V_{th} defines the shear velocity of chip.

$$V_s = v_x(h) - v_x(0) = V\frac{\cos\gamma_0}{\cos(\phi - \gamma_0)} \tag{6}$$

According to the continuity condition, Eq. 5, the chip velocity is obtained.

$$V_c = V\frac{\sin\phi}{\cos(\phi - \gamma_0)} \tag{7}$$

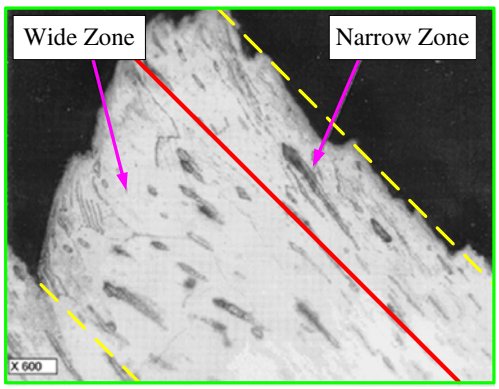

Fig. 2 Micrograph of a single chip fragment of AISI 303 [11]

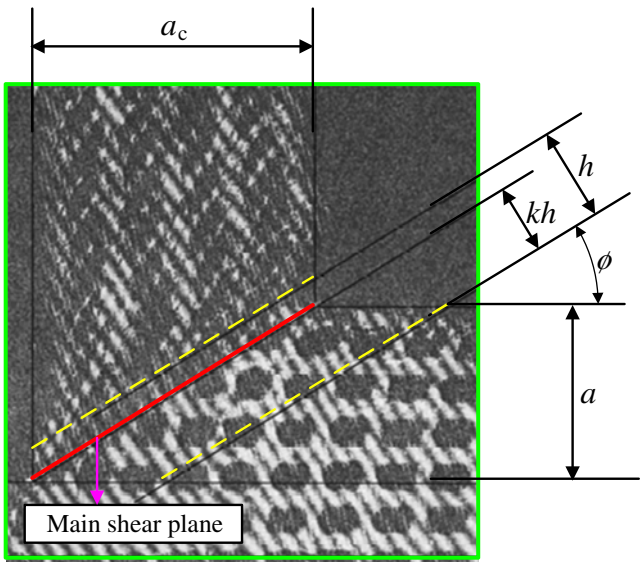

Fig. 3 Quick-stop micrograph from cutting steel [18]

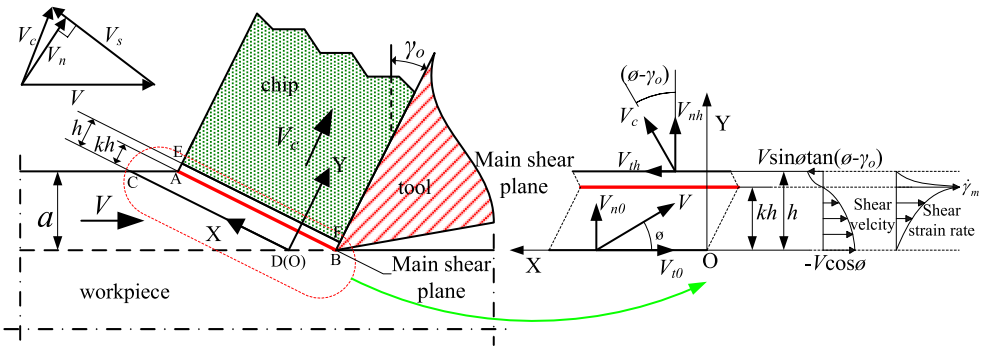

Fig. 4 Unequal division shear-zone model

The relationship of three velocities V, V_s, V_c is shown in Fig. 4.

4 Governing equations

4.1 Material constitutive equation

In order to obtain reliable results from metal cutting simulations, it is necessary to determine the properties of the workpiece material. These input data include physical and thermal data, friction and heat transfer, and most importantly the flow stress of the workpiece material under high strain (up to 4), strain rate ($10^4 \sim 10^6$ s^{-1}) and temperature (up to 1,000°C) condition that proximately exist during the cutting process. Some material models have been proposed and are respectively follow as: Johnson–Cook; Zerilli-Armstrong; Oxley; Maekawa et al.; Marusich et al. That predictions from the JC material model are closed to those obtained from the Oxley model in most case, based on the sensitivity analysis performed by Fang [19]. Nowadays, JC model is commonly used as flow stress model of work material in modeling machining operations due to its accuracy and simplicity. This material model is given as:

$$\tau = \frac{1}{\sqrt{3}}\left[A + B\left(\frac{\gamma}{\sqrt{3}}\right)^{n}\right]\left[1 + C\ln\left(\frac{\dot{\gamma}}{\dot{\gamma}_0}\right)\right]\left[1 - \left(\frac{T - T_r}{T_m - T_r}\right)^{m}\right] \tag{8}$$

Where γ is the shear plastic strain, $\dot{\gamma}$ is the shear stain rate, $\dot{\gamma}_0$ is reference plastic strain rate, T_m is melting temperature of the work material, T is instantaneous temperature of the workpiece material and T_r is room temperature or initial workpiece temperature. The constant A is yield strength (MPa), B is hardening modulus (MPa), C is strain rate sensitivity coefficient (viscosity), n is hardening coefficient, m is thermal softening coefficient. The first term in square bracket of JC equation is elastic–plastic term and represents stain hardening; the second term is viscosity term and shows that flow stress increases when material is loaded with high strain rate; the third term is thermal softening term and reflects the well-known fact that the flow stress of material decreases as temperature increases.

We know from Eq. 1 that the shear stress distributions of primary shear zone is obtained as long as the distribution condition of the shear strain, shear strain rate, and temperature are obtained.

4.2 Governing equations of strain, strain rate, and shear velocity

The strain rate, strain, shear velocity distribution of the material flow through the primary shear zone are analyzed, and the temperature and flow stress are computed iteratively. The chip formation is supposed to occur mainly by shearing in the primary shear zone, the metal does not deform until it reaches the primary shear zone. The primary shear zone is modeled as a shear band of constant thickness, a reasonable mean value for its thickness is about h=0.025 mm [20]. The main shear plane is inclined to the workpiece surface at an angle corresponding to the shear angle $ø$. In the model, the undeformed chip thickness is thin compared with its width of cut, and the chip is formed under approximately plane strain conditions. The cutter is considered as a rigid body and its edge is assumed as being perfectly sharp. The cutting edge is parallel to the workpiece surface and perpendicular to the cutting direction. The workpiece material is supposed to be homogeneous and isotropic, and governed by JC constitutive equation.

The compatibility condition relates the shear strain rate and velocity field.

$$\dot{\gamma} = \frac{\partial v_x}{\partial y} + \frac{\partial v_y}{\partial x} = \frac{\mathrm{d}v_x}{\mathrm{d}y} \tag{9}$$

The shear strain rate is also the material derivative of the shear strain.

$$\dot{\gamma} = \frac{\mathrm{d}\gamma}{\mathrm{d}t} = \frac{\partial\gamma}{\partial t} + \frac{\partial\gamma}{\partial y}\frac{\partial y}{\partial t} = V_n\frac{\partial\gamma}{\partial y} = V\sin\phi\frac{\mathrm{d}\gamma}{\mathrm{d}y} \tag{10}$$

Where t is time.

In the tests performed by Oxley [2], the strain rate increased with an increase in cutting speed and had a maximum value occurred at AB. The strain rate at entry boundary between the shear zone and workpiece and the exit boundary between the shear zone and chip is about zero. Figure 5a shows the distribution of maximum shear strain in chip formation zone. But Oxley did not give the governing law of the strain rate in the primary shear zone. A description of velocity relationship with Eq. 11 can be found in Astakhov et al. [11]. However, the derived Eq. 12 by combining Eq. 9 with Eq. 11, shows that the strain rate increase monotonically from the entry boundary to exit boundary, which is inconsistent with Oxley's test results, as shown Fig. 5b.

$$v_x = -V_{t0} + V_s\left(\frac{y}{h}\right)^{q+1} \tag{11}$$

$$\dot{\gamma} = \frac{(q+1)V_s}{h^{q+1}} y^q \tag{12}$$

Tounsi et al. [12] adopted a piecewise linear distribution of the shear strain rate as Eq. 13 according to Oxley's test. Under the assumption, there is still a large deviation between the derived velocity distribution and Astakhov's, as shown Fig. 5c. Oxley's test results also show a non-linear change tendency of the shear strain rate.

$$\dot{\gamma} = \begin{cases} \dfrac{\dot{\gamma}_m}{kh} y & y \in [0, kh] \\ \dfrac{\dot{\gamma}_m}{(1-k)h}(h-y) & y \in [kh, h] \end{cases} \tag{13}$$

Where $\dot{\gamma}_m$ is the maximum strain rate.

According to the above discussions, a piecewise power law distribution assumption of the shear strain rate, Eq. 14, is proposed in this paper as depicted in Fig. 5b. The velocity distribution derived from Eq. 14 is closer to the velocity change rate for Astakhov's division principle, as shown Fig. 5c. In addition, it can reflect the effect of cutting velocity on the strain rate.

$$\dot{\gamma} = \begin{cases} \dfrac{\dot{\gamma}_m}{(kh)^q} y^q & y \in [0, kh] \\ \dfrac{\dot{\gamma}_m}{(1-k)^q h^q}(h-y)^q & y \in [kh, h] \end{cases} \tag{14}$$

Where q is a parameter (power) characterizing the non-uniform distribution of the tangential velocity in the deformation zone. In the machining of ductile materials at low cutting speeds q=3 and at high cutting speed q=7.

Equations 9 and 14 can be combined and integrated with respect to y, using the boundary conditions that the shear strain is zero at the entry boundary of primary shear zone. So the relationship between the velocity and strain is obtained:

$$v_x = V\sin(\phi)\gamma - V\cos\phi \tag{15}$$

Equations (10) and (14) can be combined and integrated with respect to y. The shear strain distribution is then given by:

$$\gamma = \begin{cases} \dfrac{\dot{\gamma}_m}{(q+1)V\sin\phi(kh)^q} y^{q+1} & y \in [0, kh] \\ -\dfrac{\dot{\gamma}_m}{(q+1)V\sin\phi(1-k)^q h^q}(h-y)^{q+1} + \dfrac{\cos\gamma_0}{\cos(\phi-\gamma_0)\sin\phi} & y \in [kh, h] \end{cases} \tag{16}$$

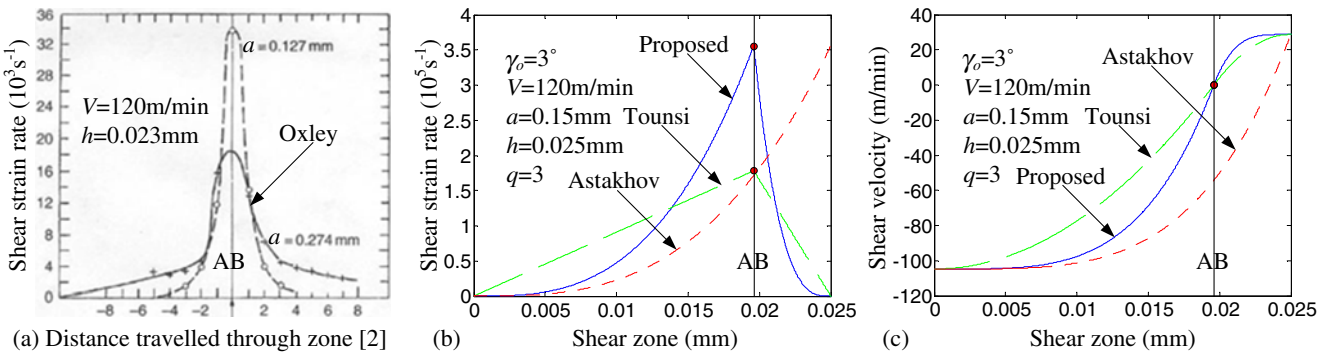

Fig. 5 Comparison of the proposed Eq. 14 with Oxley's experiment results, Eqs. 12 and 13

By replacing Eq. 14 into 9 and integrating with regard to the variable y, the boundary conditions of the velocity field, Eq. 4, is used to obtain the result. The tangential velocity component of the velocity field can be expressed as:

$$v_x = \begin{cases} \dfrac{\dot{\gamma}_m}{(q+1)(kh)^q} y^{q+1} - V\cos\phi & y \in [0, kh] \\ -\dfrac{\dot{\gamma}_m}{(q+1)(1-k)^q h^q} (h-y)^{q+1} + V\sin\phi\tan(\phi-\gamma_0) & y \in [kh, h] \end{cases} \tag{17}$$

Compared the tangential component of the cutting velocity at the entry boundary with the tangential component of chip velocity at the exit boundary, we notice a change of its sign. The main shear plane is assumed to be the plane where the tangential velocity is equal to zero [12].

$$\begin{aligned} v_x\Big|_{y=kh} &= \left(\frac{\dot{\gamma}_m}{(q+1)(kh)^q} y^{q+1} - V\cos\phi\right)\Big|_{y=kh} \\ &= \left(-\frac{\dot{\gamma}_m}{(q+1)(1-k)^q h^q} (h-y)^{q+1} + V\sin\phi\tan(\phi-\gamma_0)\right)\Big|_{y=kh} \\ &= 0 \end{aligned} \tag{18}$$

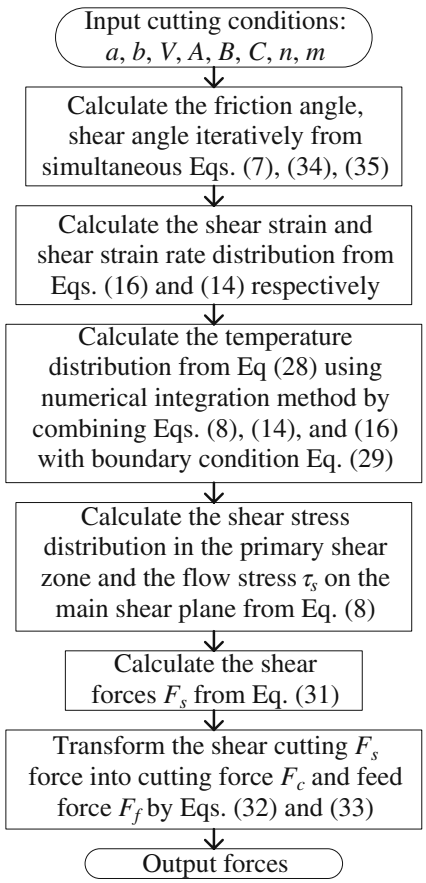

Fig. 6 Flow chart for the unequal division shear-zone model applied to orthogonal cutting

The solutions of Eq. 18 are expressed as follow:

$$k = \frac{\cos\phi\cos(\phi-\gamma_0)}{\cos\gamma_0} \tag{19}$$

$$\dot{\gamma}_m = \frac{(q+1)V\cos\gamma_0}{h\cos(\phi-\gamma_0)} \tag{20}$$

Replacing Eqs. 19 and 20. into Eqs. 14, 16, and 17, the shear strain rate, shear strain, and shear velocity distribution of the primary shear zone are obtained.

To summarize, the solutions of Eqs. 14, 16, and 18 can be calculated for some particular cases where y is equal to 0, kh, and h.

$$\begin{cases} \gamma = 0 \\ \dot{\gamma} = 0 \\ v_x = -V\cos\phi \end{cases} \quad \text{at} \quad y = 0 \tag{21}$$

$$\begin{cases} \gamma = \dfrac{k\cos\gamma_0}{\sin\phi\cos(\phi-\gamma_0)} \\ \dot{\gamma} = \dfrac{(q+1)V\cos\gamma_0}{h\cos(\phi-\gamma_0)} \\ v_x = 0 \end{cases} \quad \text{at} \quad y = kh \tag{22}$$

$$\begin{cases} \gamma = \dfrac{\cos\gamma_0}{\sin\phi\cos(\phi-\gamma_0)} \\ \dot{\gamma} = 0 \\ v_x = V\sin\phi\tan(\phi-\gamma_0) \end{cases} \quad \text{at} \quad y = h \tag{23}$$

Using the parallel-sided shear model, the shear strain and shear strain rate may be expressed as:

$$\gamma_h = \frac{\cos\gamma_0}{\sin\phi\cos(\phi-\gamma_0)} \tag{24}$$

$$\dot{\gamma}_h = \frac{V_s}{h} = \frac{V\cos\gamma_0}{h\cos(\phi-\gamma_0)} \tag{25}$$

The average shear strain rate is expressed as by Eq. 14.

$$\dot{\gamma}_a = \frac{\int_0^h \dot{\gamma}\mathrm{d}y}{h} = \frac{V\cos(\gamma_0)}{h\cos(\phi-\gamma_0)} \tag{26}$$

Table 1 Material constant of Johnson–Cook flow stress model [12, 16]

Material	A(MP)	B(MP)	C	n	m	$\dot{\gamma}_0(1/s)$	T_m(K)	T_r(K)
42CrMo4	612	436	0.008	0.15	1.46	0.001	1,800	300
316L	514	514	0.042	0.508	0.533	0.001	1,800	300

Distinction and correlation are reached by contrasting the Eqs. 22, 23, and 24: the shear strain obtained by the unequal division shear-zone model at the exit boundary is equal to that obtained by the parallel-sided shear-zone model, and the shear strain at the main shear plane is the k time of that at the exit boundary. The following conclusion can be drawn by comparing the Eqs. 22, 25, and 26: the average shear strain rate obtained by the unequal division shear-zone model is equal to that obtained by the parallel-sided shear-zone model, and the maximum shear strain rate at the main shear plane is the $q+1$ times of the average shear strain rate.

4.3 Governing equations of temperature

The workpiece is considered as a semi-infinite body, and the heat transfer process occurring during orthogonal machining is governed by the two-dimensional heat transfer equation. In the cutting process, the boundary on the shear band is usually considered adiabatic [21], the thermal conductivity is negligible and the volumetric heat generated by conduction is equal to zero. If the friction in the primary shear is neglected, the volumetric heat generation rate will be caused by the plastic deformation only. Since the temperature only depends on the coordinate y under the condition of the steady flow, assuming that a fraction μ (Taylor–Quinney coefficient) of the plastic work is converted into heat, consequently, the heat transfer equation becomes

$$\rho c V_n \frac{\partial T}{\partial y} = \mu \tau \dot{\gamma} \tag{27}$$

Where ρ, c, and μ represent the material density, the heat capacity, and the Taylor–Quinney coefficient, respectively.

After some algebraic manipulation, the Eq. 27 can be expressed as following form.

$$\frac{\mathrm{d}T}{\mathrm{d}y} = \frac{\mu}{\rho c V \sin\phi} \tau \dot{\gamma} \tag{28}$$

Table 2 Thermo-physical properties of workpiece material

Material	Density (kg/m^3)	Thermal conductivity (W/(m K))	Heat capacity (J/(kg K))
42CrMo4	7,800	54	500
AISI 316L	7,500	500	14.6

The material behavior and thermomechanical evolution in the shear zone are governed by the Eqs. 8, 14, 16, and 28. γ and $\dot{\gamma}$ are the function of y, and τ is the function of y and T, which is known from Eq. 1. So Eq. 28 is a first-order ordinary differential equations for the unknowns T and y. The equation can be easily solved by numerical integration methods, the temperature distribution is obtained. Replacing the results to Eq. 8, the shear stress distribution and the flow

Table 3 Cutting conditions for 42CrMo4 (b=3 mm)

Test number	Rake face γ_0(°)	Cutting velocity V(m/min)	Cutting thickness a(mm)
1	−5	60	0.10
2	−5	60	0.15
3	−5	120	0.10
4	−5	120	0.15
5	−5	240	0.10
6	−5	240	0.15
7	−5	480	0.10
8	−5	480	0.15
9	−3	60	0.10
10	−3	60	0.15
11	−3	120	0.10
12	−3	120	0.15
13	−3	240	0.10
14	−3	240	0.15
15	−3	480	0.10
16	−3	480	0.15
17	0	60	0.10
18	0	60	0.15
19	0	120	0.10
20	0	120	0.15
21	0	240	0.10
22	0	240	0.15
23	0	480	0.10
24	0	480	0.15
25	3	60	0.10
26	3	60	0.15
27	3	120	0.10
28	3	120	0.15
29	3	240	0.10
30	3	240	0.15
31	3	480	0.10
32	3	480	0.15

Table 4 Cutting conditions for AISI 316L (γ_0=0, b=2 mm))

Test number	1	2	3	4	5	6	7	8	9
Cutting velocity V(m/min)	67.2	67.2	67.2	128.4	128.4	128.4	187.2	187.2	187.2
Cutting thickness a(mm)	0.1	0.2	0.3	0.1	0.2	0.3	0.1	0.2	0.3

stress at the main shear plane can be also obtained. In addition, the problem has only one solution when use is made of a boundary condition. The thermal boundary conditions have to be specified: The chip temperature at the entry boundary is equal to the initial workpiece temperature or room temperature.

$$T\big|_{y=0} = T_w \tag{29}$$

5 Cutting force calculation

The shear stress distribution on the main shear plane is considered as uniform. Then the shear force F_s is proportional to the shear stress τ_s on the main shear plane. τ_s is given by the Eq. 8, a is the thickness of cut, b is the width of cut, then:

$$F_s = \frac{ab}{\sin\phi}\tau_s \tag{31}$$

The cutting force F_c and feed force F_f are easily obtained from F_s.

$$F_c = \frac{F_s\cos(\beta-\gamma_0)}{\cos(\phi+\beta-\gamma_0)} \tag{32}$$

$$F_f = \frac{F_s\sin(\beta-\gamma_0)}{\cos(\phi+\beta-\gamma_0)} \tag{33}$$

The shear angle ϕ in these relations can be calculated with the Merchant's formula. Although Merchant's formula was based on the rigid perfectly plastic assumption, Childs [22] has documented by numerous numerical experiments that varying strain rate hardening and particularly thermal softening characteristics do not lead to changed friction and

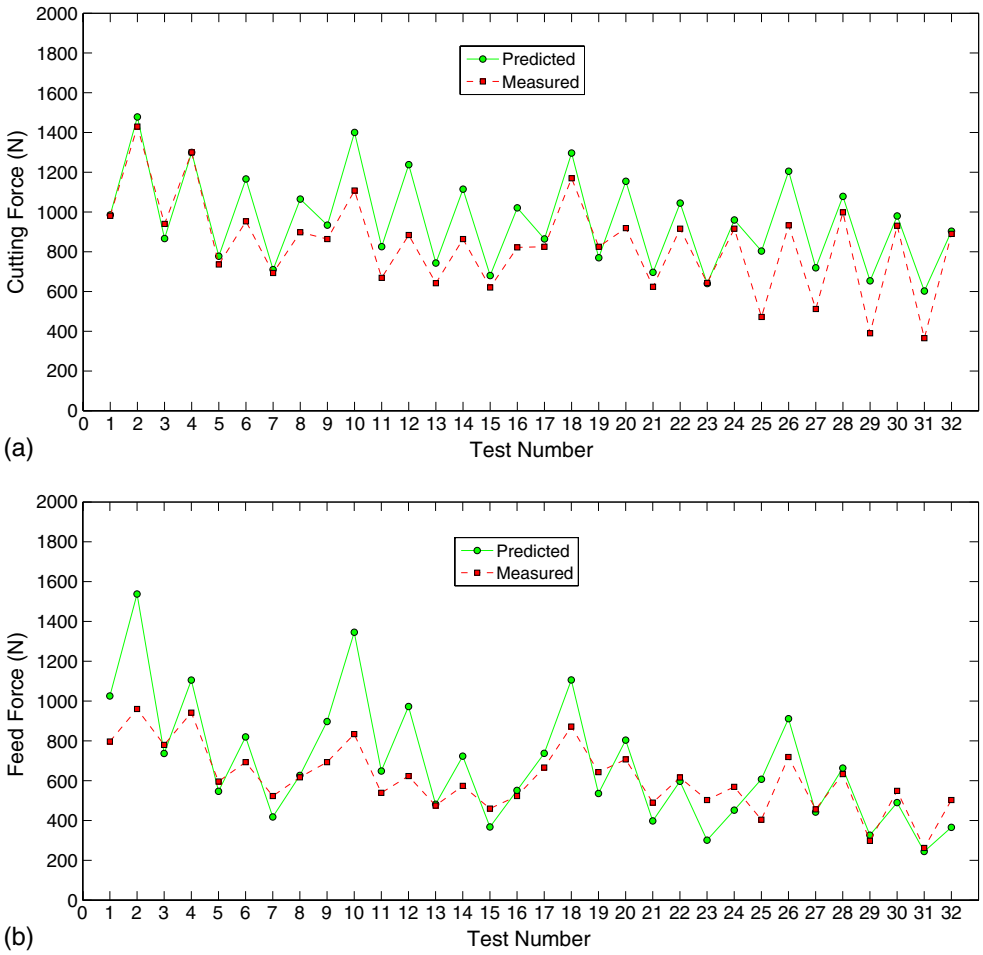

Fig. 7 Comparison of predicted cutting force and feed force with the experimental data of Moufki et al. [16] for 42CrMo4

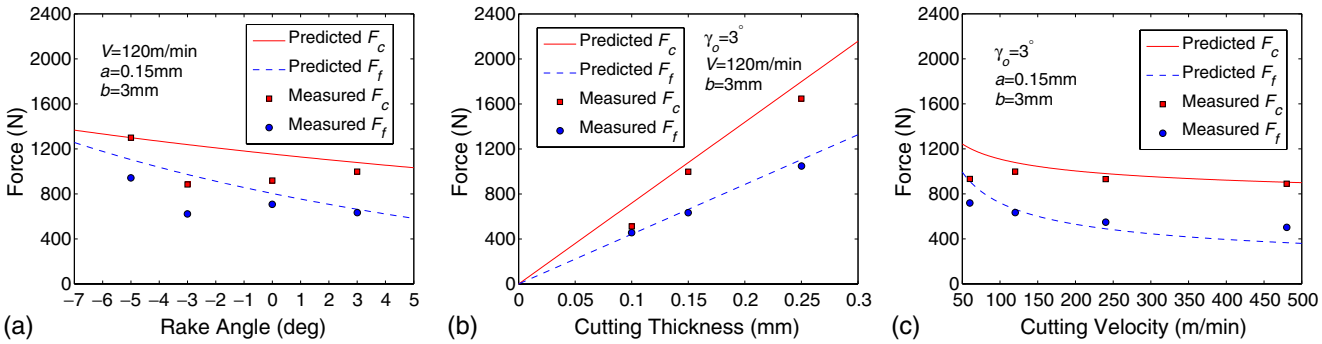

Fig. 8 Comparison between predicted and measured forces for 42CrMo4 versus rake angle (**a**), feed rate (**b**), and cutting velocity (**c**)

shear angle relationships. Here, we calculated the shear angle values approximately using simply Merchant's formula.

$$\phi = \frac{\pi}{4} - \frac{\beta}{2} + \frac{\gamma_0}{2} \tag{34}$$

As suggested by Schulz [13], the mean friction coefficient may be a power function of the chip velocity.

$$f = f_0 V_c^p \tag{35}$$

With f_0=const, p<0.

Therefore, the associated friction angle at the tool-chip interface is defined by:

$$\beta = \arctan(f) = \frac{F_{fc}}{F_{nc}} \tag{36}$$

Where F_{fc} is the friction force parallel to the rake face, F_{nc} is normal force perpendicular to the rake face. The procedure in Fig. 6 was used to determine the cutting force.

6 Results and discussions

A computer program in Matlab 7.0 is developed to carry out the analysis. The effectiveness of the proposed method is verified by the experimental data of orthogonal cutting test published by Moufki et al. [16] for 42CrMo4 and Tounsi et al. [12] for AISI 316L. Johnson–Cook flow stress data and thermo-physical properties of workpiece material are given in Tables 1 and 2. Other parameters need to be input: h=0.025 mm, q=3, μ=0.85, T_w=300K, f_0=0.704, p=−0.248. Tables 3 and 4 show the cutting conditions for cutting force measurement tests.

6.1 42CrMo4 steel validation

Figure 7 shows the comparison of cutting force and feed force for 42CrMo4 steel with experimentally measured forces of Moufki et al. In general, one can notice good agreements between the experimental and predicted cutting forces. There is a small amount of amplitude discrepancy for some cutting conditions. The main causes of the severe discrepancy between the theoretical and experimental results are accounted for:

1. Effects of tool edge radius. The predicted forces are calculated assuming that the tool edge is perfectly sharp. Nevertheless, practically all cutting tools have some finite edge radius. The blunt cutting edge contributes some amount of ploughing force. The projection of ploughing force in the direction of feed force is greater than that in the direction of cutting

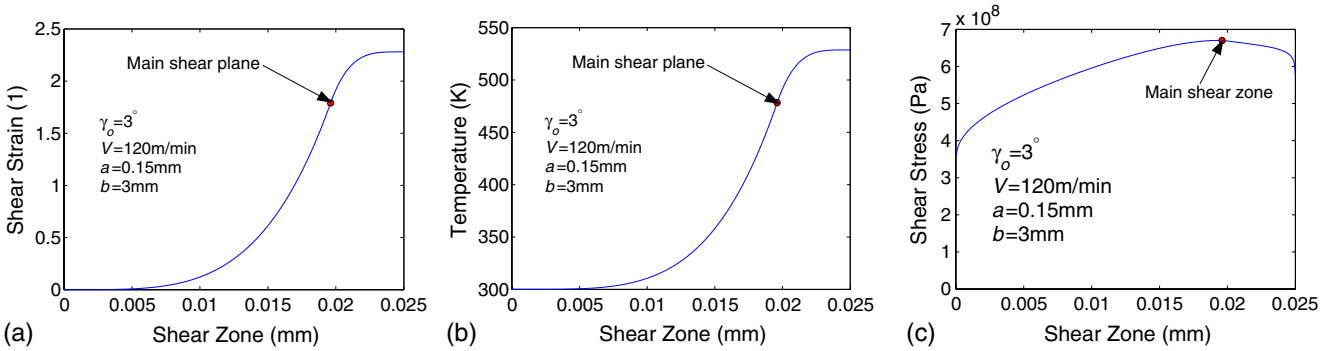

Fig. 9 Predicted results of the shear strain (**a**), temperature (**b**), and shear stress (**c**) distribution in the primary shear zone

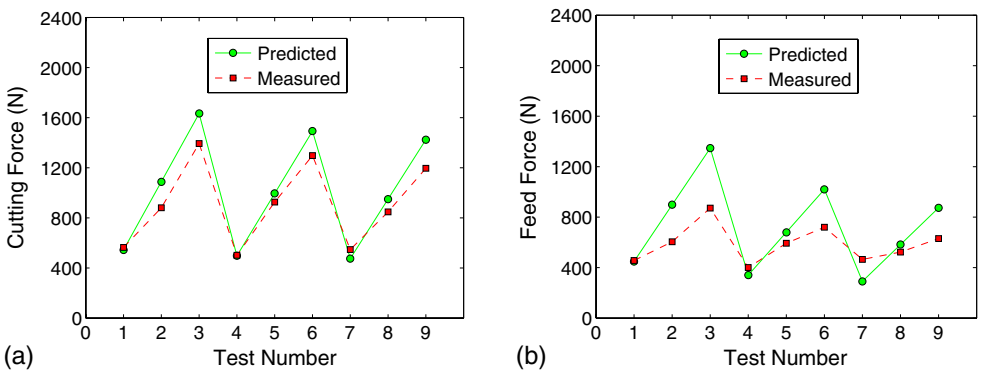

Fig. 10 Comparison of predicted cutting force (**a**) and feed force (**b**) with the experimental data of Tounsi et al. [12] for AISI 316L

force, so the deviations between the predicted and measured feed force are greater. When the cutting thickness is far smaller than the radius of the cutting edge, the ploughing force is dominant and the proposed model must be modified.

2. Friction effects. The mean friction angle that can be defined by mean friction coefficient controls the orientation of the force exerted by tool on the chip. The mean friction coefficient depends on the chip velocity, temperature and normal stress at the tool-chip interface. However, the empirical relation, Eq. 35, only takes account of the chip velocity. With the increase of cutting thickness, the cutting process generates more heat, which leads to a temperature rise at the tool-chip interface, then the mean friction coefficient reduces. Even the discrepancy between the predicted and measured feed force for some cutting conditions such as No. 2 and No. 10 is up to 60% of the measured value.
3. Effects of shear angle. In the shear angle theories, many equations were proposed, but it is still unclear which equation is most suitable. The shear angle is calculated with the Merchant's formula assuming that the workpiece is perfectly plastic, which explains the small discrepancy observed here.
4. Effects of shear zone thickness. Since it is difficult to measure the thickness of the shear zone accurately under the different conditions of machining, this paper used a typical value, h=0.025 mm. In fact, the shear zone thickness becomes wider with the increase of cutting thickness. Kececioglu [23] measured h in the range of speed 40–250 m/min, and his results show that h is approximately one quarter of the cutting thickness. Tounsi et al. [12] drew the conclusion that the shear band thickness is approximately one half of the cutting thickness based on geometrical analysis of quick-stop micrograph from cutting experiments.

As depicted in Fig. 8, the cutting forces are influenced by cutting parameters as well as tool geometry. The influence of these parameters on the force components is analyzed as follows:

1. Rake angle γ_0. An increase in the rake face angle makes the force components diminish, see Fig. 8a. This tendency is in agreement with the results of Oxley [2] and Moufki et al. [16]. The angle γ_0 influences the forces F_c and F_f through the shear angle ϕ. The shear angle increases with increase of tool rake angle, which is derived from Eq. 34. The influence sensibility of rake angle on the cutting forces weakens as the cutting speed increase.
2. Cutting thickness a. Note that in present case that tool cutting edge angle is 90º, the feed is equal to the cutting thickness. Taking no account of the influence of the cutting thickness on the friction, the increase of cutting force is proportionate to that of cutting chip thickness, as shown in Fig. 8b. Really, the increase of the cutting thickness generates more heat, which leads to a decrease of the mean friction coefficient at the tool-chip interface, then the cutting force decreases again. Based on a comprehensive consideration of two factors,

Table 5 AISI 316 flow stress data of Johnson–Cook constitutive mode [25]

Number	Author	A	B	C	n	m	$\dot{\gamma}_0$
M1	Chandrasekaran et al.	305	1,161	0.01	0.61	0.517	1
M2	Chandrasekaran et al.	305	441	0.057	0.1	1.041	1
M3	M'Saoubi	301	1,472	0.09	0.807	0.623	0.001
M4	Changeux et al.	280	1,750	0.1	0.8	0.85	200
M5	Tounsi er al.	514	514	0.042	0.508	0.533	0.001

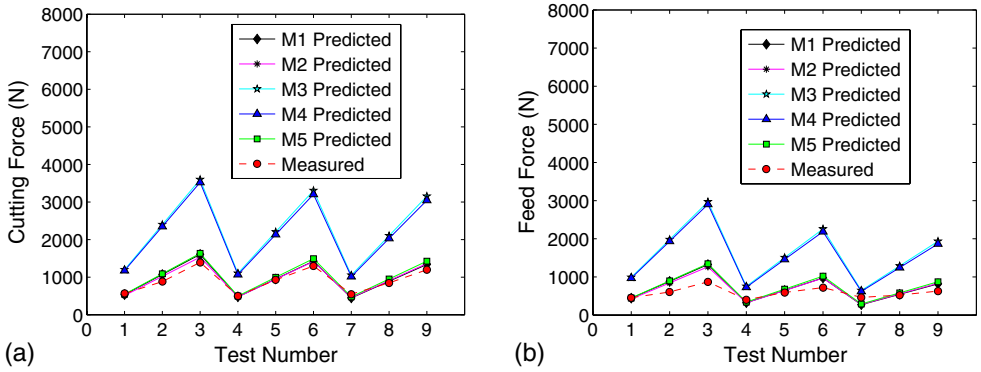

Fig. 11 Comparison between experiments [12] and predictions obtained from five different sets of flow stress data

the increase of cutting force is disproportionate to that of cutting thickness.

3. Cutting speed *V*. In the range of medium speed, the cutting force decrease when the cutting speed increase, as Fig. 8c shows. Due to the increase of the cutting speed, the temperature at tool-chip interface rises, consequently friction coefficient reduces as well as friction angle. The cutting force decreases with the decrease of shear angle which resulted from the reduction of the friction angle.

In the cutting process, the workpiece material becomes the chip mainly by shearing within the primary deformation zone. The evolution of workpiece material is very complex under high strain, high strain rate, and high temperature conditions. It is necessary to make an analysis of the distribution of shear strain, shear stress, and temperature in the deformation zone. Figure 9a shows the evolution of the shear strain. The shear strain is equal to zero at the entry boundary where the workpiece elastic deformation occurs. At the exit boundary where the material deformation is plastic, the shear strain is maximal and the chip reaches its maximum deformation. Between two boundaries, the material experiences a gradual transition from elastic to plastic deformation stage with increase of the shear strain. Figure 9b shows the changes in temperature. The temperature rises when the shear strain increase, which is attributed to the plastic deformation work generate more energy with the increase of the shear strain. The chip temperature rises by about 200°C through the shear zone, which is in good agreement with Komanduri and Hou's results [21]. Similar results are also found in Jaspers's literature [24]. Shear stress distribution in Fig. 9c shows a trend of first increase and then decrease with the chip strain and temperature increasing, which is up to a maximum value on the main shear plane. One possible reason is that the rise of temperature has more influence of thermal softening than work hardening of strain increase on the workpiece material.

6.2 AISI 316L validation

Figure 10 shows the comparison of cutting force and feed force for AISI 316L steel with experimentally measured forces of Tounri et al. [12]. The predicted values are closer to the measured values, which is attributed to the accurate and reliable flow stress data. Johnson–Cook flow stress data of 42CrMo4 steel was obtained through quasi-static and high strain rate compression test by Molinari and Moufki, and that of AISI 316L was identified through cutting test by Tounsi et al.

The flow stress data of the workpiece material is extremely crucial for the analytical prediction. Table 5 lists

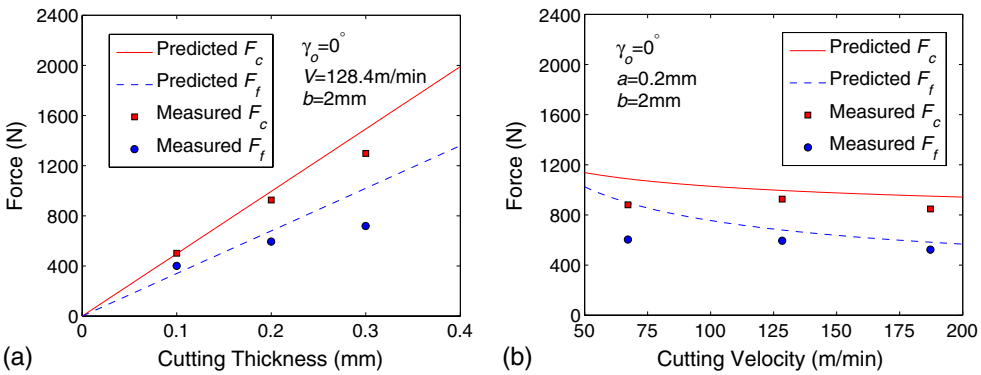

Fig. 12 Comparison between predicted and measured forces for 316L versus feed (**a**) and cutting velocity (**b**)

five different sets of workpiece material flow stress data used in the Johnson–Cook's constitutive equation from the published literature [25]. For each of the five sets of workpiece flow stress data, both experimental and predicted force components are shown in Fig. 11. Obviously, that the predicted forces of the flow stress data M1 and M4 agree well with the experimental ones, the same conclusion follows from Umbrello's FE results [25]. However, the predicted results of M2 underestimate the force components, and the predicted results of M3 and M4 are greater than the experimental ones, which are just opposite to Umbrello's FE results. Possible reasons for the apparent difference could be that Tounsi's work are identified through machining test (important in this case the role of the JC term which include the effect of the temperature), this also partly the case in Chandrasekaran [26] who identified the flow stress data using both the results from split Hopkinson's bar tests and those orthogonal slot milling experiments. This is not the case for the other sets of workpiece material flow stress data, which are identified only through high-speed deformation tests where the range of strain, strain rate, and temperature appears to be limited. The results also demonstrate that the discrepancy is different to analytical models and FE models for the same sets of flow stress data.

Figure 12 shows the influence of cutting thickness and cutting velocity on the force components for AISI 316L, the model prediction agrees well with the experiment results in trend.

7 Conclusions

In this study, an analytical method based on the unequal division shear-zone model is proposed to study the machining predictive theory in orthogonal cutting. The proposed model modifies the previous idea of the equal division shear zone. To establish the governing equation of chip flow through the primary shear zone, a piecewise power law distribution assumption of the shear strain rate is introduced. In computing the flow stress, the strain, strain rate, and temperature effects are taken into consideration. Orthogonal cutting test data for two materials namely 42CrMo4 and AISI 316L from the available literature is used for verifying the present work and agreed reasonably with the experimental results. The deviation of model prediction from experimental values was discussed to improve our work in future. For the same sets of flow stress data, the results indicate that the discrepancy is different to analytical models and FE models. The proposed model requires only workpiece material properties and cutting conditions, and is capable of predicting the cutting forces, stress distribution, and temperature distribution. It can easily extend to other workpiece material and machining operations such as oblique cutting and milling.

Acknowledgement This work is supported by the National Basic Research (973) Program of China (Grant No. 2009CB724306).

References

1. Ding TC, Zhang DS, Wang YW, Zhu XL (2010) Empirical models and optimal cutting parameters for cutting forces and surface roughness in hard milling of AISI H13 steel. Int J Adv Manuf Technol 3:18–28
2. Oxley PLB (1989) Mechanics of machining. Ellis Horwood, Chichester
3. Adetoro OB, Wen PH (2010) Prediction of mechanistic cutting force coefficients using ALE formulation. Int J Adv Manuf Technol 46:79–90
4. Third Wave AdvantEdge^{TM} (2006) Third Wave system Inc., Minneapolis, USA.
5. Merchant ME (1944) Basic mechanics of the metal cutting process. ASME J Appl Mech 66:168–175
6. Merchant ME (1945) Mechanics of the metal cutting process. J Appl Phys 16(5):267–275
7. Oxley PLB (1961) A strain-hardening solution for the shear angle in orthogonal metal cutting. Int J Mech Sci 3:68–79
8. Oxley PLB, Welsh MJM (1963) Calculating the shear angle in orthogonal metal cutting from fundamental Stress, strain, strain rate properties of the work material. In: Proceedings of the 4th International Machine Tool Design and Research Conference, Oxford. pp. 73–86.
9. Adibi-Sedeh AH, Madhavan V, Bahr B (2003) Extension of Oxley's analysis of machining to use different material models. J Manuf Sci Eng 125:656–666
10. Lalwani DI, Mehta NK, Jain PK (2009) Extension of Oxley's predictive machining theory for Johnson and Cook flow stress model. J Mater Process Technol 209:5305–5312
11. Astakhov VP, Osman MOM, Hayajneh MT (2001) Re-evaluation of the basic mechanics of orthogonal metal cutting: velocity diagram, virtual work equation, and upper bound theorem. Int J Mach Tools Manuf 41:393–418
12. Tounsi N, Vincenti J, Otho A, Elbestawi MA (2002) From the basics of orthogonal metal cutting toward the identification of the constitutive equation. Int J Mach Tools Manuf 42(2):1373–1383
13. Dudzinski D, Molinari A (1997) A modelling of cutting for viscoplastic materials. Int J Mech Sci 39(4):369–389
14. Ozlu E, Budak E, Molinari A (2007) Thermomechanical modeling of orthogonal cutting including the effect of stick-slide regions on the rake face. In: Proceedings of the 10th CIRP international workshop on modeling of machining operations, Calabria, Italy
15. Johnson W, Mellor PB (1983) Engineering plasticity. Wiley, New York
16. Moufki A, Devillez A, Dudzinski D, Molinari A (2004) Thermomechanical modelling of oblique cutting and experimental validation. Int J Mach Tools Manuf 44:971–989
17. Grzesik W (2008) Advanced machining processes of metallic materials. Elsvier, London
18. Leopold J (1999) Mechanical and physical models of machining. In: Proceedings of the 2th CIRP international workshop on modeling of machining operations, Nantes, France. pp. 24–25.
19. Fang N (2005) A new quantitative sensitivity analysis of the flow stress of 18 engineering materials in machining. J Eng Mater Technol 9:192–196
20. Shaw MC (1984) Metal cutting principles. Oxford University Press, Oxford

21. Komanduri R, Hou ZB (2000) Thermal modeling of the metal cutting process, part I: temperature rise distribution due to shear plane heat source. Int J Mech Sci 42:1715–1752
22. Childs THC (1998) Material property needs in modeling metal machining. In: Proceedings of the 1th CIRP international workshop on modeling of machining operations, Atlanta. pp. 193–202.
23. Kececioglu D (1958) Shear strain rate in metal cutting and its effect on shear flow stress. Trans ASME 80:158
24. Jaspers SPFC, Dautzenberg JH, Taminiau DA (1998) Temperature measurement in orthogonal metal cutting. Int J Adv Manuf Technol 14:7–12
25. Umbrello D, Saoubi RM, Outeiro JC (2007) The influence of Johnson-Cook material constants on finite element simulation of machining of AISI 316L steel. Int J Mach Tools Manuf 47:462–470
26. Chandrasekaran H, Saoubi RM, Chazal H (2005) Modelling of material flow stress in chip formation process from orthogonal milling and split Hopkinson bar test. Mach Sci Technol 9:131–145